December 3, 2010

Solid-State 91Zr NMR Spectroscopy Studies of Zirconocene Olefin Polymerization Catalyst Precursors

Aaron J. Rossini, *University of Windsor*
Ivan Hung, *University of Windsor*
Samuel A. Johnson, *University of Windsor*
Carla Slebodnick, *Virginia Polytechnic Institute and State University*
Mike Mensch, *Virginia Polytechnic Institute and State University*, et al.

THE JOURNAL OF PHYSICAL CHEMISTRY Letters

pubs.acs.org/JPCL

Solid-State $^{47/49}$Ti NMR of Titanocene Chlorides

Aaron J. Rossini, Ivan Hung,† and Robert W. Schurko*

Department of Chemistry and Biochemistry, University of Windsor, Windsor, Ontario, Canada

ABSTRACT Magic angle spinning (MAS) and static $^{47/49}$Ti solid-state NMR (SSNMR) spectra of the cyclopentadienyl (Cp) titanium chloride compounds, Cp_2TiCl_2 (**1**), $Cp^*_2TiCl_2$ (**2**) [Cp* = C_5Me_5], $CpTiCl_3$ (**3**), and Cp^*TiCl_3 (**4**) have been acquired at magnetic field strengths of 21.1 and 9.4 T. From these spectra, it is possible to measure anisotropic $^{47/49}$Ti NMR interaction parameters, which are extremely sensitive to differences in molecular structure. At a magnetic field of 21.1 T, the $^{47/49}$Ti spectra can be acquired efficiently with standard echo pulse sequences. Quantum chemical calculations of $^{47/49}$Ti electric field gradient (EFG) and chemical shielding (CS) tensor parameters are presented. The theoretical EFG and CS tensor orientations are utilized to relate the anisotropic NMR tensor parameters to the molecular and electronic structures of the complexes.

SECTION Kinetics, Spectroscopy

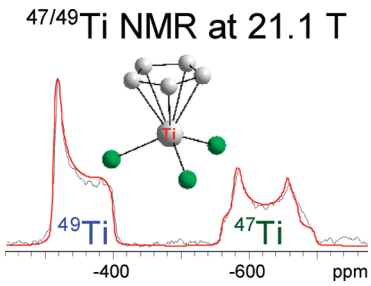

Early transition-metal metallocene complexes are highly active catalysts for olefin polymerization, affording better control over the stereospecificity and molecular weight distributions of resulting polymers than the traditional heterogeneous $TiCl_4/MgCl_2$ Ziegler−Natta system.[1−4] While certain metallocenes can be dissolved in polymerization media and used as homogeneous catalysts, they are also employed as heterogeneous catalysts on support materials such as alumina and silica.[2,4] The solubilized homogeneous catalysts are amenable to traditional structural, kinetic, and mechanistic studies; however, the active sites of supported catalysts are often difficult to characterize.[2,4] One intriguing possibility for characterizing heterogeneous catalysts is solid-state NMR (SSNMR) spectroscopy of quadrupolar nuclei.[5−10] We have demonstrated that SSNMR spectra of metal quadrupolar nuclei that lie at the "hearts" of metallocenes can act as sensitive probes of molecular structure and dynamics[11−14] and could therefore find use for characterizing heterogeneous catalysts. In this regard, $^{47/49}$Ti SSNMR could potentially serve as a powerful probe of molecular structure for titanocene-based heterogeneous catalysts.

Titanium possesses two NMR-active nuclei, ^{47}Ti (I = 5/2) and ^{49}Ti (I = 7/2),[15] both of which are unreceptive owing to their low natural abundances [n.a.(^{47}Ti) = 7.44 %, n.a.(^{49}Ti) = 5.41 %], moderate quadrupole moments [Q(^{47}Ti) = 29.0 fm^2, Q(^{49}Ti) = 24.0 fm^2], and low gyromagnetic ratios [γ(^{47}Ti) = -1.5105×10^7 rad s^{-1} T^{-1}, γ(^{49}Ti) = -1.51095×10^7 rad s^{-1} T^{-1}].[15] ^{49}Ti is preferred for SSNMR experiments as the central transition (CT) powder patterns are significantly narrower due to its slightly smaller quadrupole moment and higher nuclear spin. However, the similarity of the gyromagnetic ratios of ^{47}Ti and ^{49}Ti complicates the acquisition and analysis of SSNMR spectra; the difference of the Larmor frequencies is so small that the ^{49}Ti and ^{47}Ti resonances are located ∼267 ppm apart, which often results in overlapping CT powder patterns. Despite these difficulties, there are numerous examples of $^{47/49}$Ti solution[16−30] and solid-state[31−53] NMR found in the literature, reflecting the myriad number of important systems containing titanium. To date, most $^{47/49}$Ti SSNMR studies have been restricted to oxides and other extended solids. In this work, we report the first application of $^{47/49}$Ti SSNMR for the structural characterization of molecular titanium-containing complexes. Before complex solid catalysts can be investigated by SSNMR of quadrupolar nuclei such as $^{47/49}$Ti, fundamental studies on well-characterized crystalline species are required. To this end, we have acquired MAS and static $^{47/49}$Ti SSNMR spectra of the titanocenes, **1**−**4**. Quantum chemical calculations of NMR tensor parameters are also presented.

Magic angle spinning (MAS) $^{47/49}$Ti SSNMR spectra of compounds **1**−**4** acquired at 21.1 T are shown in Figure 1. At 21.1 T, spectra of **1**, **3**, and **4** could be acquired in relatively short experimental times (< 1.5 h). The spectrum of **2** required ∼32000 scans (1 day) due to the increased breadth of its MAS powder pattern and the reduced Ti content. The ^{49}Ti MAS spectra of **1** and **2** display characteristic second-order quadrupolar CT powder patterns, indicative of sizable quadrupolar interactions. From the simulations of these patterns, it is possible to obtain C_Q, η_Q, and δ_{iso} (Table 1). For both **1** and **2**, the ^{47}Ti powder patterns are obscured due to their comparably larger breadths and subsequently lower signal-to-noise ratios. Simulations of the ^{47}Ti powder patterns, which utilize a C_Q(^{47}Ti) that has been scaled by the ratio of ^{47}Ti and ^{49}Ti quadrupole moments, indicate that much faster sample spinning speeds are necessary to prevent sideband overlap. For this reason, the reported $^{47/49}$Ti NMR tensor parameters are based on simulations of the MAS ^{49}Ti CT powder patterns, with the MAS ^{47}Ti CT patterns providing additional constraints on these parameters. It should be noted

Received Date: August 24, 2010
Accepted Date: September 16, 2010
Published on Web Date: September 24, 2010

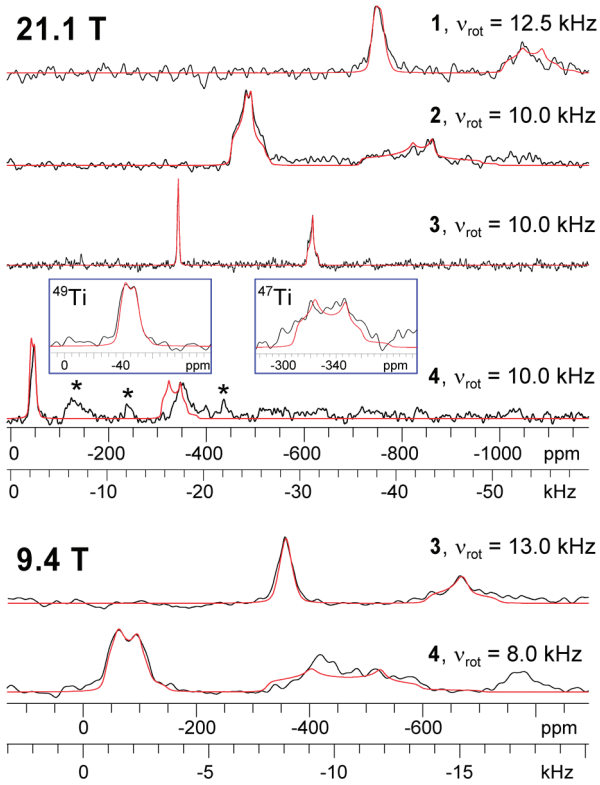

Figure 1. Experimental MAS $^{47/49}$Ti SSNMR spectra (black traces) of **1** (Cp_2TiCl_2), **2** ($Cp^*_2TiCl_2$), **3** ($CpTiCl_3$), and **4** (Cp^*TiCl_3) acquired at 21.1 T [$\nu_0(^{49}Ti)$ = 50.75 MHz] and spectra of **3** and **4** acquired at 9.4 T [$\nu_0(^{49}Ti)$ = 22.53 MHz]. Sample spinning speeds are given in the figure. Analytical simulations are overlaid on the experimental spectra (red traces). All spectra at 21.1 T were acquired with a standard rotor synchronized 90−180° echo pulse sequence. Asterisks denote spinning sidebands. The inset of the spectrum of **4** shows the ^{47}Ti and ^{49}Ti isotropic peaks that are obtained when the spinning sidebands are added onto the isotropic peak. Spectra at 9.4 T were acquired with the DFS−echo (**3**) and DFS−QCPMG (**4**) pulse sequences. The spectrum of **4** at 9.4 T was formed by co-adding the QCPMG echoes in the time domain, followed by Fourier transformation of the resultant echo. Additional experimental details are provided in the Supporting Information.

that the crystal structure of **1** contains two crystallographically distinct titanium sites with similar local environments.[54] As a result, the $^{47/49}$Ti NMR spectrum of **1** is composed of two very similar powder patterns which can be simulated with a single set of quadrupolar and chemical shift parameters. Quantum chemical calculations also confirm the similarities between the sites (vide infra).

In comparison to **1** and **2**, the MAS $^{47/49}$Ti CT powder patterns of the trichloride species, **3** and **4**, are relatively narrow, and at 21.1 T, it is difficult to accurately extract values of C_Q and η_Q. The ^{47}Ti powder patterns of **3** and **4** are slightly broader and can be used to estimate C_Q and η_Q, although with large uncertainties. In order to obtain accurate measurements of C_Q and η_Q for **3** and **4**, additional MAS spectra were recorded at 9.4 T (Figure 1, bottom). The CT powder patterns are considerably broader than those obtained at 21.1 T and exhibit features typical of a strong second-order quadrupolar interaction. From these spectra, EFG tensor parameters of C_Q = 1.6 MHz and η_Q = 0.95 and C_Q = 3.0 MHz and η_Q = 0.35 were obtained for **3** and **4**, respectively, comparable to the small $C_Q(^{95}Mo)$ values observed for a similar "piano-stool" complex, $(Me_3C_6H_3)Mo(CO)_3$.[55] Experimental times at 9.4 T were significantly greater than those at 21.1 T. The MAS $^{47/49}$Ti SSNMR spectrum of **3** was acquired in 2 h (3680 scans, 2 s pulse delay) with a DFS−echo pulse sequence, while the spectrum of **4** was acquired in ∼21 h (25000 scans, 3 s pulse delay) with a DFS−QCPMG sequence.

Complex **4** possesses a relatively large $^{47/49}$Ti chemical shift anisotropy (CSA, vide infra), which further disperses spectral intensity into the spinning sidebands and affects the shape of the isotropic CT pattern; therefore, it is necessary to add the sideband intensity into the isotropic position to obtain an undistorted CT pattern (inset, Figure 1).[56] The spectrum of **4** at 9.4 T does not require the addition of spinning sidebands into the isotropic pattern due to an increase in the relative magnitude of the quadrupolar interaction with respect to the CSA.

The trends in the titanium isotropic chemical shifts mirror those observed in previous solution NMR studies.[17−19,23−26,30] An increase in δ_{iso} is observed for the Cp* complexes in comparison to the analogous Cp complexes, and the mono-Cp′ species possess higher chemical shifts than the bis-Cp′ species (Cp′ refers to a Cp ligand of any substitution pattern). The differences in δ_{iso} of **3** and **4** have previously been correlated with the absorption maxima (λ_{max}) of UV−visible spectra, which are 380 and 437 nm for **3** and **4**, respectively.[26,30] It is well-known that smaller energy separations between occupied and virtual orbitals give rise to larger paramagnetic shielding interactions and hence more positive chemical shifts (increased deshielding).[57−63] Thus, correlations between δ_{iso} and λ_{max} are observed when the MOs that make large contributions to the nuclear magnetic shielding are the same MOs involved in optical transitions.

A comparison of the $^{47/49}$Ti EFG tensor parameters obtained from solid-state and solution $^{47/49}$Ti NMR experiments is not as straightforward. In solution, the values of C_Q are estimated from the full widths at half-height (FWHH) of the $^{47/49}$Ti peaks, under the approximation of the extreme narrowing limit. Furthermore, the values of η_Q cannot be accurately determined from solution NMR spectra (many instances of predicting C_Q values from FWHHs rely on the assumption that η_Q = 0, which is most often not the case). Nonetheless, the previously measured FWHH values from solution $^{47/49}$Ti NMR spectra of **1**−**3** correlate well with the relative magnitudes of C_Q obtained from the corresponding SSNMR spectra, and the values of $C_Q(^{49}Ti)$ are slightly larger for the bis-Cp′ species in comparison to those of the mono-Cp′ species.[18,26,30] However, FWHH values obtained from solution NMR spectra of **4** suggest that it possesses a smaller C_Q than that of **3**,[18,30] which is not the case in the solid state. Both **3** and **4** possess very small quadrupolar coupling constants; therefore, the differences in the magnitude of C_Q may be a result of subtle structure deviations and/or long-range intermolecular electrostatic interactions. We note that our research group has previously observed that substituted sodocenes and niobocenes possess larger values of $C_Q(^{23}Na)$ and $C_Q(^{93}Nb)$, respectively, than the corresponding unsubstituted Cp complexes.[12,64] However, given the limitations of the

DOI: 10.1021/jz1012017 | J. Phys. Chem. Lett. 2010, 1, 2989–2998

Table 1. Experimental and Calculated $^{47/49}$Ti EFG and CS Tensor Parameters

complex/method/structure	$\delta_{iso}(^{49}Ti)$ (ppm)[a]	$C_Q(^{49}Ti)$ (MHz)[b]	η_Q[b]	Ω (ppm)[c]	κ[c]	α (°)[d]	β (°)	γ (°)
Cp_2TiCl_2 (**1**)/experiment	**−732(5)**	**4.2(4)**	**0.45(30)**	**275(50)**	**0.65(30)**	**20(70)**	**20(20)**	**−10(90)**
1/RHF/site 1 ideal Cp[e]	−689	−6.1	0.21	166	0.7	63	82	9
1/RHF/site 1 X-ray[e]	−737	−2.0	0.55	252	0.2			
1/RHF/site 2 ideal Cp	−692	−6.0	0.16	168	0.7			
1/RHF/site 2 X-ray	−715	4.2	0.95	230	0.3			
1/B3LYP/site 1 ideal Cp	−678	3.8	0.16	526	−0.3			
1/B3LYP/site 1 X-ray	−729	7.8	0.07	588	−0.4			
1/B3LYp/site 2 ideal Cp	−680	3.8	0.12	530	−0.3			
1/B3LYP/site 2 X-ray	−708	8.3	0.04	576	−0.3			
$Cp^*_2TiCl_2$ (**2**)/experiment	**−449(4)**	**5.5(3)**	**0.72(10)**	**165(60)**	**−0.1(8)**	**80(40)**	**90(30)**	**−5(60)**
2/RHF/ideal Cp	−478	−5.9	0.40	101	−0.1	154	19	37
2/RHF/X-ray	−479	−6.5	0.42	138	−0.4			
2/B3LYP/ideal Cp	−399	−4.0	0.67	327	−0.1			
2/B3LYP/X-ray	−401	6.4	0.83	317	0.1			
$CpTiCl_3$ (**3**)/experiment	**−341(2)**	**1.6(2)**	**0.95(10)**	**85(10)**	**0.8(2)**	**50(30)**	**12(12)**	**10(40)**
3/RHF/ideal Cp	−200	3.8	0.46	44	−0.5			
3/RHF/X-ray	−214	3.8	0.60	43	−0.2	71	86	171
3/B3LYP/ideal Cp	−239	8.5	0.19	375	−0.8			
3/B3LYP/X-ray	−253	8.5	0.24	369	−0.8			
Cp^*TiCl_3 (**4**)/experiment	**−33(3)**	**3.0(3)**	**0.35(10)**	**650(75)**	**0.9(3)**	**30(90)**	**0(10)**	**0(90)**
4/RHF/ideal Cp	−33	1.2	0.62	394	0.9	43	63	26
4/RHF/X-ray	−33	1.4	0.57	414	1.0			
4/B3LYP/ideal Cp	−33	2.6	0.77	102	0.7			
4/B3LYP/X-ray	−33	2.1	0.62	138	0.7			
Cp_2TiMe_2 (**5**)/experiment								
Cp_2TiMe_2/RHF/ideal Cp	−218	22.5	0.79	1809	−1.0			
Cp_2TiMe_2/RHF/X-ray	−234	25.5	0.84	1811	−1.0			

[a] The shifts are referenced to neat $TiCl_4(l)$ [$\delta_{iso}(^{49}Ti) = 0.0$ ppm] via a secondary external standard of solid $SrTiO_3$, for which $\delta_{iso}(^{49}Ti) = -843$ ppm. The value is $\delta_{iso}(^{47}Ti) = \delta_{iso}(^{49}Ti) - 267$ ppm. Calculated isotropic magnetic shielding (MS) values (σ_{iso}) were converted to δ_{iso} values by subtracting the calculated MS values from those calculated for **4**, $\delta_{iso} = \sigma_{iso}(\mathbf{4}) - \sigma_{iso}(\text{complex}) - 33$ ppm. [b] The EFG tensor is defined by three principal components ordered such that $|V_{11}| \leq |V_{22}| \leq |V_{33}|$ where, $C_Q = eQV_{33}/h$ and $0.0 \leq \eta_Q = (V_{11} - V_{22})/V_{33} \leq 1.0$. The value is $C_Q(^{47}Ti) = 1.21\,C_Q(^{49}Ti)$. [c] The CS tensor is described by three principal components ordered such that $\delta_{11} \geq \delta_{22} \geq \delta_{33}$ where, $\delta_{iso} = (\delta_{11} + \delta_{22} + \delta_{33})/3$, $\Omega = \delta_{11} - \delta_{33}$, and $\kappa = 3(\delta_{22} - \delta_{iso})/\Omega$. [d] The Rose convention is used to describe the Euler angles. Uncertainties associated with the last digits of the experimental NMR parameters are given in parentheses. [e] Quantum chemical calculations employed atomic coordinates obtained from single-crystal X-ray diffractions structures. The "X-ray" and "ideal Cp" labels indicate whether XRD coordinates of the Cp carbon atoms were employed or whether idealized Cp rings were employed (see main text).

approximations described above, it is more likely that the solid-state measurement of C_Q is simply more accurate. For complexes **1**, **2**, and **4**, η_Q values are not close to either 0 or 1, indicating that all of the components are distinct from one another. For **3**, η_Q is close to 1, indicating that V_{11} is the distinct component of the EFG tensor and $V_{22} \approx -V_{33}$.

The values of $C_Q(^{49}Ti)$ obtained for **1**−**4** are on the smaller end of the range previously measured from SSNMR spectra of non-cubic oxides and other extended solids, where $C_Q(^{49}Ti)$ is found to range from 2.6 to 24.0 MHz.[44] Similarly, in our ^{91}Zr SSNMR study of bis-Cp zirconocene dihalide complexes, we found that $C_Q(^{91}Zr)$ was relatively small compared to those of oxides and related systems (unpublished results; publication forthcoming).[11] This indicates that the ground-state electronic environment at the metal atoms in d^0 metallocene halide complexes is of comparatively higher spherical symmetry than that of the metal oxides.

Titanium CSA has previously been observed for several titanates (Ω = 22−180 ppm)[44] and the rutile phase of TiO_2 (Ω = 30 ppm).[50] Furthermore, our previous ^{91}Zr SSNMR studies of zirconocenes,[11] ^{45}Sc SSNMR study of coordination complexes,[65] and extensive ^{51}V SSNMR studies of Polenova et al.[66−70] have indicated that CSAs are substantial for the nuclei of the elements directly adjacent to Ti in the periodic table. In order to measure the CS tensor parameters, the span (Ω), and skew (κ), static $^{47/49}$Ti SSNMR spectra of **1**−**4** were acquired at 21.1 and 9.4 T (Figure 2). The static spectra also serve to confirm EFG tensor parameters isolated from MAS spectra and allow for the determination of the Euler angles which describe the relative orientation of the EFG and CS tensors in each complex.

The appearance of the static spectra is indicative of the presence of substantial titanium CSA (Figure 2); it is not possible to simulate the static powder patterns using only the quadrupolar interaction (Figure S1, Supporting Information).

DOI: 10.1021/jz1012017 | J. Phys. Chem. Lett. 2010, 1, 2989–2998

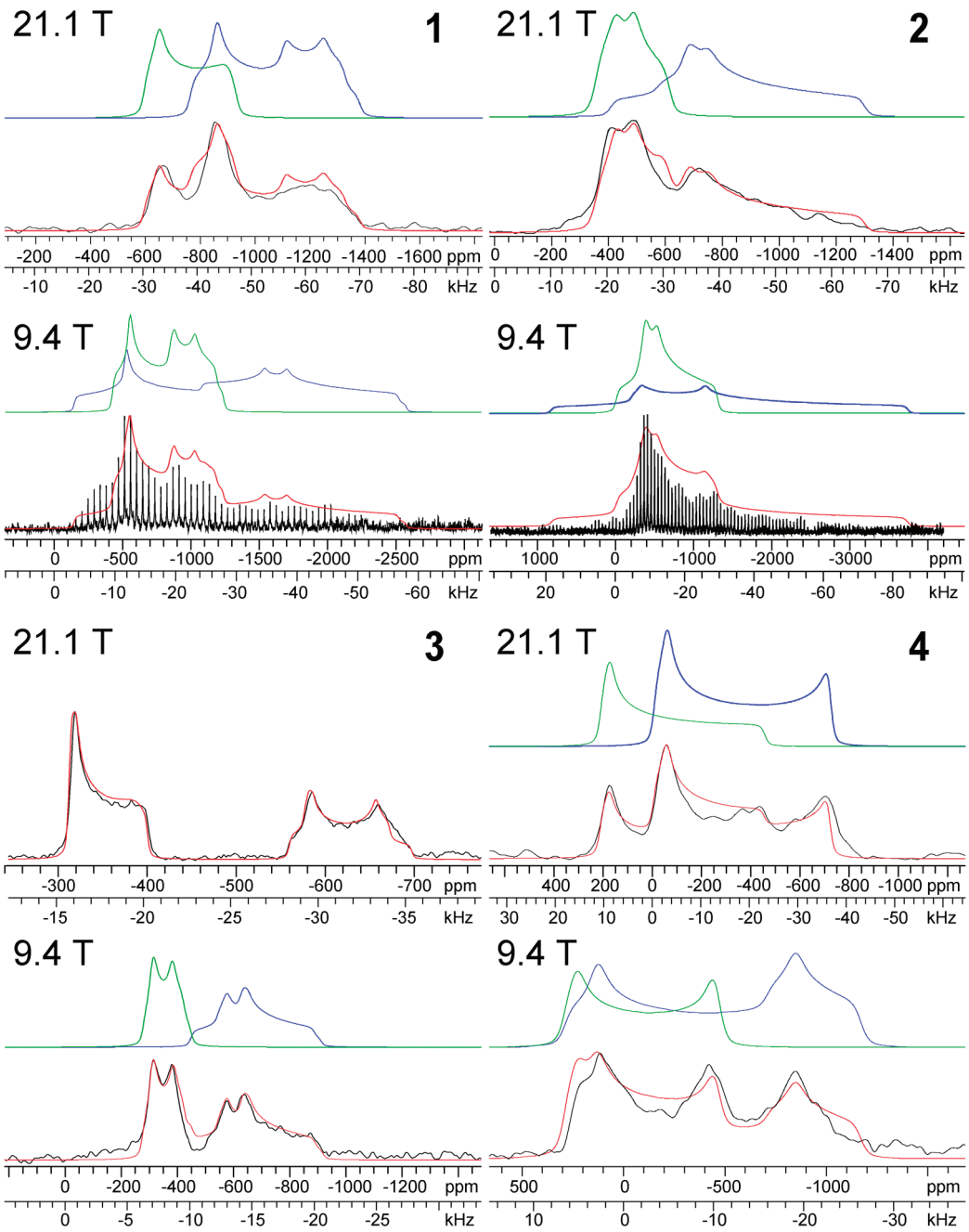

Figure 2. Static $^{47/49}$Ti SSNMR spectra of **1** (Cp_2TiCl_2), **2** ($Cp^*_2TiCl_2$), **3** ($CpTiCl_3$), and **4** (Cp^*TiCl_3) acquired at 21.1 and 9.4 T. Analytical simulations (red traces) are overlaid on the experimental spectra (black traces). Deconvolutions of the ^{49}Ti (green traces) and ^{47}Ti (blue traces) powder pattern simulations are also shown. Spectra at 21.1 T were acquired with a standard echo sequence. Spectra of **1** and **2** at 9.4 T were acquired with the DFS−QCPMG pulse sequence.

For all static spectra, the ^{47}Ti and ^{49}Ti powder patterns are observed to overlap, except for the spectrum of **3** acquired at 21.1 T. Overlap of the patterns can complicate simulations of the static spectra; however, with spectra from two magnetic fields, it is possible to obtain reasonably accurate measurements of the CS tensors. If more accurate measurements of the CS tensors and Euler angles are desired, QCPMG experiments which employ pulses with nutation angles designed to give a spectrum with only one of the $^{47/49}$Ti nuclei may be employed.[50] However, acquisition times for the static spectra were significantly longer than those for the MAS spectra due to much wider dispersion of the signal intensity in the former. At 21.1 T, static echo spectra were acquired in 3−20 h, while at 9.4 T, DFS−echo and DFS−QCPMG pulse sequences were used, with experiment times on the order of days.

From the static spectra, Ω is found to range from 85 (**3**) to 650 ppm (**4**). The Ω of **1** is greater than that of **2** (Cp vs Cp*), while for **3** and **4**, the opposite is observed. The value of Ω for

DOI: 10.1021/jz1012017 | J. Phys. Chem. Lett. 2010, 1, 2989–2998

4 is substantially larger than those of the other complexes, as well as those previously reported for other systems ($\Omega \leq$ 180 ppm).[44] As mentioned above, the MAS spectrum of **4** possesses a number of intense spinning sidebands not observed in any of the other MAS spectra, consistent with this large CSA. SIMPSON simulations of the $^{47/49}$Ti MAS spectra with variable values of Ω confirm the unusually large value of Ω = 650 ppm (Figure S2, Supporting Information).

The values of κ are close to +1 for **1**, **3**, and **4**, indicating that the CS tensors are all nearly axially symmetric (i.e., $\delta_{11} \approx \delta_{22}$, and δ_{33} is the distinct component of each CS tensor). Axial symmetry of the CS tensor is expected for **3** and **4**, given that these complexes possess pseudo-C_3 rotational axes. This is similar to the κ values near +1 measured for the ^{55}Mn and ^{95}Mo SSNMR spectra of piano-stool arene−metal complexes.[55,71] However, it is interesting to note that for a series of bis-Cp zirconocene dihalide complexes analogous to **1** and **2**, we have found that κ is always close to −1 (a full discussion of this is beyond the scope of this paper; unpublished results). For **2**, κ = −0.1, which indicates that the three principal components of the CS tensor are unequal and approximately evenly spaced, although there is large uncertainty associated with the experimental value of κ. In summary, titanium CSA is found to be relatively large for **1**−**4**, and distinct values of Ω are observed for each complex, suggesting that this parameter can act as a useful secondary probe of molecular structure.

Results from the quantum chemical calculations of titanium EFG and magnetic shielding (MS) tensors are shown in Table 1. We note that quantum chemical calculations provide the principal components of the MS tensor (σ_{ii}), which can then be converted to CS tensor parameters for comparison to experimental results (see footnote of Table 1). All atomic coordinates (except those for H atoms) for calculations were taken from the previously determined single-crystal X-ray diffraction structures. In addition, we have performed calculations with atomic coordinates which employ "idealized" Cp rings. In these calculations, the crystallographically determined Cp centroid distances have been retained; however, perfectly planar Cp rings with ideal C−C bond lengths (1.40 Å) and C−C−C angles (108°) have been employed. We have found this approach necessary to obtain accurate quantum chemical calculations of ^{91}Zr EFG tensor parameters of zirconocenes (unpublished results). A number of methods and basis set combinations were tested for both sets of coordinates, which are summarized in the Supporting Information (Tables S1−S4). In general, RHF and B3LYP calculations, which employ the Ahlrichs valence double-ζ polarized (pVDZ) basis set,[72] on Ti give the best agreement between experiment and theory, although calculations of some EFG and CS tensor parameters are not satisfactory. In particular, calculated values of C_Q, η_Q, and Ω are poor for many of the complexes, regardless of whether X-ray or idealized Cp ring carbon atom positions are employed. Given the small size of the data set, it is also not clear whether the use of ideal Cp ring coordinates gives superior results to those which employ Cp ring coordinates determined by X-ray crystallography.

The RHF calculations are clearly superior for the calculation of the CS tensor parameters, yielding nearly quantitative values of δ_{iso} and correctly predicting the symmetry of the CS tensor (κ) for **1**, **2**, and **4**. While the calculations do not accurately predict the values of Ω, they do correctly predict the relative values for complexes **1**−**4** (i.e., Ω for **4** > **1** > **2** > **3**). B3LYP calculations yield accurate values of δ_{iso}; however, calculated values of Ω and κ show poor agreement with experimental values.

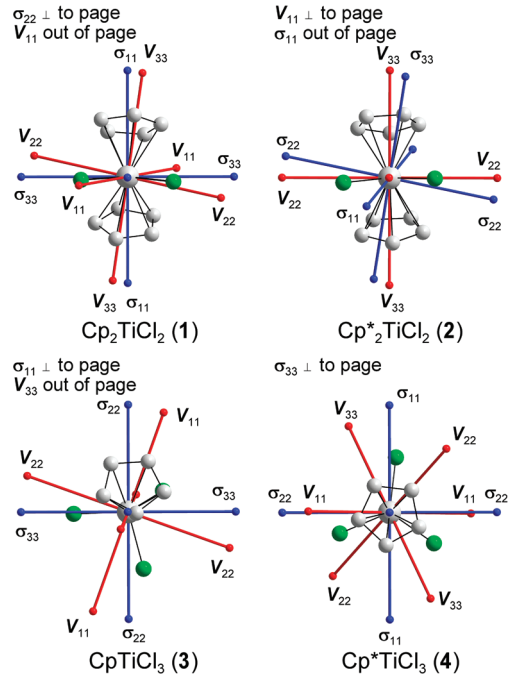

Figure 3. EFG and CS tensor orientations for **1**−**4** obtained from quantum chemical calculations. The Euler angles associated with these tensor orientations are listed in Table 1. Methyl groups and hydrogen atoms bound to the Cp rings have been omitted for clarity.

Both RHF and B3LYP calculations yield C_Q and η_Q values which show relatively poor agreement with the experimental data. The calculations are able to correctly predict that C_Q is relatively small for **1**−**4**; however, they are unable to predict the relative magnitudes of C_Q within the series. Accurate calculations of ^{45}Sc and ^{51}V EFG tensor parameters have previously been demonstrated,[65−67,69,73] and Ti is a relatively light element for which relativistic effects should be minimal. This suggests that calculations of titanium EFG tensors should be straightforward. It may be that because C_Q is relatively small for **1**−**4**, minor errors in the calculated EFG tensor principal components (V_{ii}) lead to substantial errors in both C_Q and η_Q. Periodic plane-wave DFT calculations were also attempted for **1**−**4** (Table S5, Supporting Information); however, the calculated NMR tensor parameters also show poor agreement with experiment. All of this data suggest that more quantum chemical methods and functionals should be tested in the future in order to identify suitable methods for calculations of $^{47/49}$Ti NMR tensor parameters.

Finally, we present calculated EFG and MS tensor orientations for **1**−**4** (Figure 3). The tensor orientations provide insight into the origin of the observed anisotropic NMR interactions and allow for correlations between the NMR interaction tensors

DOI: 10.1021/jz1012017 | J. Phys. Chem. Lett. 2010, 1, 2989–2998

and molecular symmetry and structure. The orientation of the calculated EFG tensors in **1** and **2** are similar. The orientation of V_{33} perpendicular to the Cl−Ti−Cl plane arises because the electric field is large in the direction of the chloride ligands but small along the direction of the Cp ligands, giving rise to the large gradient. We have previously calculated that the magnitude of V_{33} significantly increases as the Zr−Cl bond lengths of Cp_2ZrCl_2 are shortened (unpublished results). In fact, the EFG and MS tensor orientations calculated for **1** are similar to those previously calculated for Cp_2ZrCl_2. At this time, we do not comment on the orientation of the EFG tensors for **3** and **4** as the calculated values of C_Q and η_Q show relatively poor agreement with experiment, though they are shown for reference in Figure 3.

For the Cp complexes **1** and **3**, σ_{11}, the least-shielded components of the MS tensors, are oriented toward the Cp ring carbon atom which lies above the Ti atom. For **1**, σ_{11} is oriented such that it is approximately perpendicular to the Cl−Ti−Cl plane. Deshielding along this direction likely arises from mixing of high-energy occupied Ti−Cl bonding molecular orbitals with low-lying unoccupied d orbitals, both of which are located in the Cl−Ti−Cl plane. It is known that paramagnetic deshielding arises due to magnetic-field-induced mixing of occupied and virtual molecular orbitals,[57−63] and deshielding contributions are largest in the direction perpendicular to the plane of mixing. In this regard, Hoffman has previously presented Hückel calculations which demonstrate that the valence molecular orbitals in titanocenes correspond to Cl−Ti σ- and π-bonding orbitals.[74]

In **2**, the most shielded component of the MS tensor, σ_{33} is directed toward a Cp* carbon atom which lies above the Ti atom, while in **4**, σ_{33} is directed toward the centroid of the Cp* ligand. The distinct orientations of the MS tensors for **2** and **4** compared to **1** and **3** suggest that the energies and symmetries of the molecular orbitals are undoubtedly influenced by the increased basicity of the Cp* ligand in comparison to the Cp ligands. The orientations of σ_{11} and σ_{22} for both **2** and **4** suggest that deshielding primarily arises due to mixing of high-energy occupied or low-lying virtual orbitals of Ti−Cp* bonding character, which is also consistent with the observations of more positive δ_{iso} values for the Cp* complexes. As noted above, previous UV−vis measurements on **3** and **4** have found that λ_{max} occurs at longer wavelengths in the latter.[26,30] If the MOs that make large anisotropic contributions to the nuclear magnetic shielding are the same MOs involved in optical transitions, then it is anticipated that decreased energy separations between these MOs will lead to a larger titanium CSA in **4** than that in **3**.

Finally, EFG and CS tensor calculations were also performed for Cp_2TiMe_2 (**5**), which is a species important to catalytic processes involving titanocenes. In order to obtain active metallocene olefin polymerization catalysts, it is necessary to treat them with an activator or cocatalyst, such as methylaluminoxane (MAO).[2,4] MAO abstracts the chloride ligands, replaces them with methyl ligands, and subsequently abstracts a methyl group to generate a catalytically active, coordinatively unsaturated, cationic metallocene. We have previously observed that Cp_2ZrMe_2 possesses relatively large values of $C_Q(^{91}Zr)$ = 28.0 MHz and $\Omega(^{91}Zr)$ = 1750 ppm (unpublished results). Consistent with these findings, quantum chemical calculations indicate that **5** has a very large C_Q (ca. 22−25 MHz) and CSA (Ω > 1800 ppm). From these calculations, it is clear that $^{47/49}$Ti SSNMR spectra very distinct from those of **1** and **2** would be observed for methyl titanocenes. However, due to the large C_Q and Ω values, **5** would be expected to possess a wide-line $^{47/49}$Ti SSNMR spectrum of ∼300−400 kHz in breadth at 21.1 T, the acquisition of which would be difficult and beyond the scope of the current work.

MAS and static $^{47/49}$Ti SSNMR spectra were acquired for complexes **1**−**4**, each yielding unique sets of EFG and CS tensor parameters. C_Q values for these complexes are small with respect to the known range of C_Q values. All of the complexes possess significant titanium CSAs, affording another set of NMR parameters which can be used to provide insight into their molecular and electronic structures. Quantum chemical calculations can accurately predict δ_{iso} for **1**−**4**; however, further computational methods and basis sets must be evaluated in order to obtain better agreement between experimental and theoretical anisotropic $^{47/49}$Ti NMR parameters.

At an ultrahigh magnetic field of 21.1 T, it is possible to acquire MAS and static $^{47/49}$Ti SSNMR spectra in several hours with standard echo techniques. However, at a moderate magnetic field of 9.4 T, signal-enhancement techniques are required for the acquisition of $^{47/49}$Ti SSNMR spectra, and acquisition times remain on the order of days. The lengthy experiment times required to obtain adequate signal-to-noise ratios suggest that $^{47/49}$Ti SSNMR experiments on systems with low Ti contents, such as heterogeneous catalysts, would be very challenging. However, isotopic labeling in conjunction with cross-polarization (CP)-CPMG experiments at cryogenic temperatures could enable the acquisition of $^{47/49}$Ti spectra of heterogeneous catalysts. Ellis and Lipton have extensively utilized this approach to acquire SSNMR spectra of metalloproteins, which contain dilute concentrations of low-γ nuclei such as ^{25}Mg and ^{67}Zn.[75−79] CP from ^{1}H could be especially beneficial for $^{47/49}$Ti, given that the maximum theoretical signal enhancement is $\gamma_{^1H}/\gamma_{^{49}Ti}$ = −17.7. In addition, the differences in CP Hartmann−Hahn matching conditions which arise from the different spins of ^{47}Ti and ^{49}Ti could be useful for selectively exciting only one of the isotopes.[80,81] In an analogous manner to CP experiments, the development of dynamic nuclear polarization (DNP) experiments may also be very beneficial for SSNMR studies of unreceptive nuclei such as $^{47/49}$Ti as the maximum signal enhancement is $\gamma_e/\gamma_{^{49}Ti}$ = 11654.[82,83] These signal-enhancing methods and the sensitivity of $^{47/49}$Ti NMR parameters to differences in molecular structure make $^{47/49}$Ti SSNMR very appealing for continued study of such systems.

EXPERIMENTAL METHODS

Samples of **1**−**4** were purchased from Strem Chemicals Inc. and used without further purification. All samples were finely ground into powders and packed into zirconia rotors or shortened glass NMR tubes under an inert N_2 atmosphere. $^{47/49}$Ti SSNMR spectra were acquired on a 21.1 T Bruker

DOI: 10.1021/jz1012017 | J. Phys. Chem. Lett. 2010, 1, 2989–2998

Avance II NMR spectrometer at the Canadian National Ultrahigh-Field Facility and a 9.4 T Varian InfinityPlus. A complete listing of experimental details is given in the Supporting Information (Tables S6−S9). Experiments at 9.4 T were conducted with Chemagnetics 5 mm HXY MAS, 4 mm HXY, and 5 mm static probes equipped with a Chemagnetics low-γ tuning box. Experiments at 21.1 T were acquired with a Bruker 4 mm HX MAS probe and home-built single-channel static 5 mm and 7 mm probes. Pulse width calibrations were performed on saturated solutions of **1** dissolved in CH_2Cl_2. Chemical shifts were referenced to neat $TiCl_4(l)$ [$\delta_{iso}(^{49}Ti)$ = 0.0 ppm] via an external standard of powdered $SrTiO_3$ [$\delta_{iso}(^{49}Ti)$ = −843 ppm].[33] Experiments at 21.1 T employed standard echo sequences for acquisition. Experiments at 9.4 T employed DFS−echo[84,85] or DFS−QCPMG[86,87] pulse sequences for signal enhancement. The Rose convention is used to describe the direction and order of the Euler angles which describe the CS and EFG tensor orientation.[88,89] Analytical simulations of MAS and static $^{47/49}$Ti SSNMR spectra were performed with the WSolids program.[90] The SIMPSON program was employed for numerical simulations of the MAS ^{49}Ti SSNMR spectrum of **4** (Figure S2, Supporting Information).[91]

Quantum chemical calculations of NMR tensor parameters were performed with the Gaussian 03[92] software package and employed molecular coordinates for isolated molecules resolved from single-crystal X-ray diffraction structures.[54,93−95] In all cases, the hydrogen atoms were fixed to idealized positions prior to calculations. Both restricted Hartree−Fock (RHF) and hybrid density functional theory (B3LYP) calculations were performed.[96−98] Several Ti basis sets[72] were tested, and results from these calculations are given in the Supporting Information. The double-ζ basis set of Dunning[99] was employed for Cl, and the 6-311G** basis set was employed for C and H. Additional ab initio plane-wave density functional calculations were performed using the CASTEP NMR program (Table S5, Supporting Information).[100,101]

SUPPORTING INFORMATION AVAILABLE Additional quantum chemical calculation results, NMR experiment details, additional simulations of $^{47/49}$Ti SSNMR spectra, and a complete author list for Gaussian 03. This material is available free of charge via the Internet at http://pubs.acs.org.

AUTHOR INFORMATION

Corresponding Author:

*To whom correspondence should be addressed. Fax: (519) 973-7098. E-mail: rschurko@uwindsor.ca.

Present Addresses:

†Center of Interdisciplinary Magnetic Resonance, National High Magnetic Field Laboratory, 1800 East Paul Dirac Drive, Tallahassee, FL 32310, U.S.A.

ACKNOWLEDGMENT A.J.R. thanks the Natural Science and Engineering Research Council (NSERC, Canada) for a graduate scholarship. R.W.S. thanks NSERC for research funding and also acknowledges the Canadian Foundation for Innovation (CFI), the Ontario Innovation Trust (OIT), and the University of Windsor for funding the solid-state NMR facility. R.W.S. also thanks the Ontario Ministry of Research and Innovation for an Early Researcher Award. Mr Ryan W. Mills is thanked for running preliminary Gaussian 03 calculations. This work was made possible by the facilities of the Shared Hierarchical Academic Research Computing Network (SHARCNET: www.sharcnet.ca). Dr. Victor Terskikh and Dr. Shane Pawsey are thanked for assistance with experiments conducted at 21.1 T at the Canadian National Ultrahigh-Field Facility. Access to the 900 MHz NMR spectrometer was provided by the National Ultrahigh-Field NMR Facility for Solids (Ottawa, Canada), a national research facility funded by the Canada Foundation for Innovation, the Ontario Innovation Trust, Recherche Québec, the National Research Council Canada, and Bruker BioSpin and managed by the University of Ottawa (www.nmr900.ca). NSERC is acknowledged for a Major Resources Support grant.

REFERENCES

(1) Soga, K.; Shiono, T. Ziegler−Natta Catalysts for Olefin Polymerizations. *Prog. Polym. Sci.* **1997,** *22*, 1503–1546.

(2) Hlatky, G. G. Heterogeneous Single-Site Catalysts for Olefin Polymerization. *Chem. Rev.* **2000,** *100*, 1347–1376.

(3) Kaminsky, W.; Laban, A. Metallocene Catalysis. *Appl. Catal., A* **2001,** *222*, 47–61.

(4) Severn, J. R.; Chadwick, J. C.; Duchateau, R.; Friederichs, N. "Bound but not Gagged" — Immobilizing Single-Site Alpha-Olefin Polymerization Catalysts. *Chem. Rev.* **2005,** *105*, 4073–4147.

(5) Abragam, A. In *The Principles of Nuclear Magnetism*; Oxford University: New York, 1961; pp 264−353.

(6) Dye, J. L.; Ellaboudy, A. S.; Kim, J. In *Multinuclear Magnetic Resonance in Liquids and Solids — Chemical Applications*, NATO ASI Series; Granger, P., Harris, R. K., Eds.; Kluwer Aacademic Publishers: Dordrecht, The Netherlands, 1990; Vol. 322, pp 217−321.

(7) Amoureux, J. P.; Fernandez, C.; Granger, P. In *Multinuclear Magnetic Resonance in Liquids and Solids — Chemical Applications*, NATO ASI Series; Granger, P., Harris, R. K., Eds.; Kluwer Aacademic Publishers: Dordrecht, The Netherlands, 1990; Vol. 322, pp 409−424.

(8) Kentgens, A. P. M. A Practical Guide to Solid-State NMR of Half-Integer Quadrupolar Nuclei With Some Applications to Disordered Systems. *Geoderma* **1997,** *80*, 271–306.

(9) Smith, M. E.; van Eck, E. R. H. Recent Advances in Experimental Solid State NMR Methodology for Half-Integer Spin Quadrupolar Nuclei. *Prog. Nucl. Magn. Reson. Spectrosc.* **1999,** *34*, 159–201.

(10) Ashbrook, S. E.; Duer, M. J. Structural Information From Quadrupolar Nuclei in Solid State NMR. *Concepts Magn. Reson. Part A* **2006,** *28A*, 183–248.

(11) Hung, I.; Schurko, R. W. Solid-State ^{91}Zr NMR of Bis(cyclopentadienyl)dichlorozirconium(IV). *J. Phys. Chem. B* **2004,** *108*, 9060–9069.

(12) Lo, A. Y. H.; Bitterwolf, T. E.; Macdonald, C. L. B.; Schurko, R. W. Solid-State ^{93}Nb and ^{13}C NMR Investigations of Half-Sandwich Niobium(I) and Niobium(V) Cyclopentadienyl Complexes. *J. Phys. Chem. A* **2005,** *109*, 7073–7087.

(13) Widdifield, C. M.; Schurko, R. W. A Solid-State ^{39}K and ^{13}C NMR Study of Polymeric Potassium Metallocenes. *J. Phys. Chem. A* **2005,** *109*, 6865–6876.

(14) Hamaed, H.; Lo, A. Y. H.; Lee, D. S.; Evans, W. J.; Schurko, R. W. Solid-State ^{139}La and ^{15}N NMR Spectroscopy of Lanthanum-Containing Metallocenes. *J. Am. Chem. Soc.* **2006,** *128*, 12638–12639.

(15) Harris, R. K.; Becker, E. D.; De Menezes, S. M. C.; Goodfellow, R.; Granger, P. NMR Nomenclature. Nuclear Spin Properties and Conventions for Chemical Shifts (IUPAC Recommendations 2001). *Pure Appl. Chem.* **2001,** *73*, 1795–1818.

(16) Kidd, R. G.; Matthews, R. W.; Spinney, H. G. Titanium-47 and Titanium-49 Nuclear Magnetic Resonance in Titanium(IV)-Halogen Compounds. *J. Am. Chem. Soc.* **1972,** *94*, 6686–6689.

(17) Hao, N.; Sayer, B. G.; Denes, G.; Bickley, D. G.; Detellier, C.; McGlinchey, M. J. Titanium-47 and -49 Nuclear Magnetic Resonance Spectroscopy: Chemical Applications. *J. Magn. Reson.* **1982,** *50*, 50–63.

(18) Dormond, A.; Fauconet, M.; Leblanc, J. C.; Moise, C. First NMR Observation of Titanium-47 and -49 in Cyclopentadienyl Complexes. *Polyhedron* **1984,** *3*, 897–900.

(19) Gassman, P. G.; Campbell, W. H.; Macomber, D. W. An Unusual Relationship Between Titanium-49 Chemical Shift and Ti(2p3/2) Binding Energy. The Use of Titanium-49 NMR in Evaluating the Electronic Effect of Methyl Substitution on the Cyclopentadienyl Ligand. *Organometallics* **1984,** *3*, 385–387.

(20) McGlinchey, M. J.; Bickley, D. G. Titanium NMR Spectroscopy: A Comment on Some Recent Assignments. *Polyhedron* **1985,** *4*, 1147–1148.

(21) Finch, W. C.; Anslyn, E. V.; Grubbs, R. H. Substituent Effects on the Cleavage Rates of Titanocene Metallacyclobutanes. *J. Am. Chem. Soc.* **1988,** *110*, 2406–2413.

(22) Chi, K. M.; Frerichs, S. R.; Philson, S. B.; Ellis, J. E. Highly Reduced Organometallics. 23. Synthesis, Isolation, and Characterization of Hexacarbonyltitanate(2−), ($Ti(CO)_6^{2-}$). Titanium NMR Spectra of Carbonyltitanates. *J. Am. Chem. Soc.* **1988,** *110*, 303–304.

(23) Traill, P. R.; Young, C. G. Application of a Transverse NMR Probe in the Detection of Broad Titanium-49 Resonances from Titanium(IV) and Titanium(II) Compounds. *J. Magn. Reson.* **1990,** *90*, 551–556.

(24) Berger, S.; Bock, W.; Marth, C. F.; Raguse, B.; Reetz, M. T. Titanium-47,49 NMR of Some Titanium Compounds. *Magn. Reson. Chem.* **1990,** *28*, 559–560.

(25) Hafner, A.; Duthaler, R. O.; Marti, R.; Rihs, G.; Rothe-Streit, P.; Schwarzenbach, F. Enantioselective Syntheses with Titanium Carbohydrate Complexes. Part 7. Enantioselective Allyltitanation of Aldehydes with Cyclopentadienyldialkoxyallyltitanium Complexes. *J. Am. Chem. Soc.* **1992,** *114*, 2321–2336.

(26) Hafner, A.; Okuda, J. Titanium NMR Data for Some Titanium Half-Sandwich Complexes Bearing Substituted Cyclopentadienyl Ligands. *Organometallics* **1993,** *12*, 949–950.

(27) Boyle, T. J.; Alam, T. M.; Mechenbier, E. R.; Scott, B. L.; Ziller, J. W. Titanium(IV) Neopentoxides. X-ray Structures of $Ti_3(\mu_3\text{-}O)(\mu_3\text{-}Cl)(\mu\text{-}OCH_2CMe_3)_3(OCH_2CMe_3)_6$ and $[Ti(\mu\text{-}OCH_2CMe_3)(OCH_2CMe_3)_3]_2$. *Inorg. Chem.* **1997,** *36*, 3293–3300.

(28) Fedotov, M. A.; Zekovets, G. A.; Gavrilov, V. Y. Ti(IV) State in Concentrated Hydrochloric Acid Solutions as Studied by Multinuclear Magnetic Resonance. *Zh. Neorg. Khim.* **1999,** *44*, 973–976.

(29) Foris, A. ^{47,49}Ti and ^{13}C NMR Spectra of Titanium-Containing Catalysts. *Magn. Reson. Chem.* **2000,** *38*, 1044–1046.

(30) Erben, M.; Ruzicka, A.; Picka, M.; Pavlik, I. ^{47}Ti, ^{49}Ti NMR Spectra of Half-Sandwich Titanium(IV) Complexes. *Magn. Reson. Chem.* **2004,** *42*, 414–417.

(31) Forbes, C. E.; Hammond, W. B.; Cipollini, N. E.; Lynch, J. F. Nuclear Magnetic Resonances of $BaTiO_3$. *J. Chem. Soc., Chem. Commun.* **1987,** 433–436.

(32) Bastow, T. J. An NMR Study of Barium-137 and Titanium-47,-49 in Ferroelectric Barium Titanate ($BaTiO_3$). *J. Phys.: Condens. Matter* **1989,** *1*, 4985–4991.

(33) Dec, S. F.; Davis, M. F.; Maciel, G. E.; Bronnimann, C. E.; Fitzgerald, J. J.; Han, S. S. Solid-State Multinuclear NMR Studies of Ferroelectric, Piezoelectric, and Related Materials. *Inorg. Chem.* **1993,** *32*, 955–959.

(34) Bastow, T. J.; Forwood, C. T.; Gibson, M. A.; Smith, M. E. Local Site Symmetry and Electronic Structure of Trialuminide and Related Intermetallic Alloys Probed by Solid-State NMR. *Phys. Rev. B* **1998,** *58*, 2988–2997.

(35) Bastow, T. J.; Gibson, M. A.; Forwood, C. T. ^{47,49}Ti NMR: Hyperfine Interactions in Oxides and Metals. *Solid State Nucl. Magn. Reson.* **1998,** *12*, 201–209.

(36) Bastow, T. J.; Whitfield, H. J. ^{47,49}Ti NMR: Evolution of Crystalline TiO_2 from the Gel State. *Chem. Mater.* **1999,** *11*, 3518–3520.

(37) Bastow, T. J.; Doran, G.; Whitfield, H. J. Electron Diffraction and ^{47,49}Ti and ^{17}O NMR Studies of Natural and Synthetic Brookite. *Chem. Mater.* **2000,** *12*, 436–439.

(38) Koyama, T.; Sugita, H.; Wada, S.; Miyatani, K.; Tanaka, T.; Ishikawa, M. An Evidence for a Spin Gap in Copper-Thiospinel $CuTi_2S_4$. *Physica B* **2000,** *284−288*, 1513–1514.

(39) Bastow, T. J. ^{47,49}Ti NMR in Metals, Inorganics, and Gels. *Z. Naturforsch., A: Phys. Sci.* **2000,** *55*, 291–297.

(40) Gervais, C.; Smith, M. E.; Pottier, A.; Jolivet, J. P.; Babonneau, F. Solid-State ^{47,49}Ti NMR Determination of the Phase Distribution of Titania Nanoparticles. *Chem. Mater.* **2001,** *13*, 462–467.

(41) Crevoiserat, S.; Lehnert, T.; Dimitropoulos, C.; Gotthardt, R. Study of the Martensitic Phase Transformation in Ni−Ti by Nuclear Magnetic Resonance. *Metallofiz. Noveishie Tekhnol.* **2001,** *23*, 182–187.

(42) Bastow, T. J.; Whitfield, H. J. ^{137}Ba and ^{47,49}Ti NMR. Electric Field Gradients in the Non-Cubic Phases of $BaTiO_3$. *Solid State Commun.* **2001,** *117*, 483–488.

(43) MacKenzie, K. J. D.; Smith, M. E. *Multinuclear Solid-State NMR of Inorganic Materials*; Pergamon: Oxford, U.K., 2002.

(44) Padro, D.; Jennings, V.; Smith, M. E.; Hoppe, R.; Thomas, P. A.; Dupree, R. Variations of Titanium Interactions in Solid State NMR-Correlations to Local Structure. *J. Phys. Chem. B.* **2002,** *106*, 13176–13185.

(45) Ganapathy, S.; Gore, K. U.; Kumar, R.; Amoureux, J. P. Multinuclear (^{27}Al, ^{29}Si, ^{47}Ti, ^{49}Ti) Solid-State NMR of Titanium Substituted Zeolite USY. *Solid State Nucl. Magn. Reson.* **2003,** *24*, 184–195.

(46) Zalar, B.; Laguta Valentin, V.; Blinc, R. NMR Evidence for the Coexistence of Order−Disorder and Displacive Components in Barium Titanate. *Phys. Rev. Lett.* **2003,** *90*, 037601.

(47) Kiyama, T.; Fujisawa, S.; Saitoh, H.; Itoh, M.; Kodama, K.; Takigawa, M. NMR Study of Orbital Ordering in $RTiO_3$ (R = Y, Gd, and La). *Physica B* **2003,** *329*, 733–735.

(48) Kiyama, T.; Itoh, M. Presence of 3d Quadrupole Moment in $LaTiO_3$ Studied by ^{47}Ti, ^{49}Ti NMR. *Phys. Rev. Lett.* **2003,** *91*, 7202–7206.

(49) Brauniger, T.; Madhu, P. K.; Pampel, A.; Reichert, D. Application of Fast Amplitude-Modulated Pulse Trains for Signal Enhancement in Static and Magic-Angle-Spinning ^{47}Ti, ^{49}Ti-NMR Spectra. *Solid State Nucl. Magn. Reson.* **2004,** *26*, 114–120.

(50) Larsen, F. H.; Farnan, I.; Lipton, A. S. Separation of ^{47}Ti and ^{49}Ti Solid-State NMR Lineshapes by Static QCPMG Experiments at Multiple Fields. *J. Magn. Reson.* **2006,** *178*, 228–236.

DOI: 10.1021/jz1012017 | *J. Phys. Chem. Lett.* **2010,** *1*, 2989–2998

(51) Toberer, E. S.; Epping, J. D.; Chmelka, B. F.; Seshadri, R. Hierarchically Porous Rutile Titania: Harnessing Spontaneous Compositional Change in Mixed-Metal Oxides. *Chem. Mater.* **2006,** *18*, 6345–6351.

(52) Wagner, G. W.; Procell, L. R.; Munavalli, S. ^{27}Al, ^{47}Ti, ^{49}Ti, ^{31}P, and ^{13}C MAS NMR Study of VX, GD, and HD Reactions With Nanosize Al_2O_3, Conventional Al_2O_3 and TiO_2, and Aluminum and Titanium Metal. *J. Phys. Chem. C* **2007,** *111*, 17564–17569.

(53) Zhu, J. F.; Trefiak, N.; Woo, T. K.; Huang, Y. N. A $^{47/49}$Ti Solid-State NMR Study of Layered Titanium Phosphates at Ultrahigh Magnetic Field. *J. Phys. Chem. C* **2009,** *113*, 10029–10037.

(54) Clearfield, A.; Warner, D. K.; Saldarriagamolina, C. H.; Ropal, R.; Bernal, I. Structural Studies of $(\pi\text{-}C_5H_5)_2MX_2$ Complexes and Their Derivatives — Structure of Bis(π-cyclopentadienyl)Titanium Dichloride. *Can. J. Chem.* **1975,** *53*, 1622–1629.

(55) Bryce, D. L.; Wasylishen, R. E. A ^{95}Mo and ^{13}C Solid-State NMR and Relativistic DFT Investigation of Mesitylenetricarbonylmolybdenum(0) — A Typical Transition Metal Piano-Stool Complex. *Phys. Chem. Chem. Phys.* **2002,** *4*, 3591–3600.

(56) Wu, G.; Zhu, J. F.; Mo, X.; Wang, R. Y.; Terskikh, V. Solid-State ^{17}O NMR and Computational Studies of C-Nitrosoarene Compounds. *J. Am. Chem. Soc.* **2010,** *132*, 5143–5155.

(57) Grutzner, J. B. Chemical Shift Theory. Orbital Symmetry and Charge Effects on Chemical Shifts. In *Recent Advances in Organic NMR Spectroscopy*; Lambert, J. B., Rittner, R., Eds.; Norell Press: Landisville, NJ, 1987; pp 17−42.

(58) Schreckenbach, G.; Ziegler, T. Calculation of NMR Shielding Tensors Using Gauge-Including Atomic Orbitals and Modern Density-Functional Theory. *J. Phys. Chem.* **1995,** *99*, 606–611.

(59) Wiberg, K. B.; Hammer, J. D.; Zilm, K. W.; Cheeseman, J. R.; Keith, T. A. NMR Chemical Shifts. 1. The Role of Relative Atomic Orbital Phase in Determining the Sign of the Paramagnetic Terms: ClF, CH_3F, $CH_3NH_3^+$, FNH_3^+, and HC CF. *J. Phys. Chem. A* **1998,** *102*, 8766–8773.

(60) Wiberg, K. B.; Hammer, J. D.; Zilm, K. W.; Keith, T. A.; Cheeseman, J. R.; Duchamp, J. C. NMR Chemical Shifts. Substituted Acetylenes. *J. Org. Chem.* **2004,** *69*, 1086–1096.

(61) Forgeron, M. A. M.; Wasylishen, R. E. A Solid-State ^{95}Mo NMR and Computational Investigation of Dodecahedral and Square Antiprismatic Octacyanomolybdate(IV) Anions: Is the Point-Charge Approximation an Accurate Probe of Local Symmetry? *J. Am. Chem. Soc.* **2006,** *128*, 7817–7827.

(62) Feindel, K. W.; Ooms, K. J.; Wasylishen, R. E. A Solid-State ^{55}Mn NMR Spectroscopy and DFT Investigation of Manganese Pentacarbonyl Compounds. *Phys. Chem. Chem. Phys.* **2007,** *9*, 1226–1238.

(63) Widdifield, C. M.; Schurko, R. W. Understanding Chemical Shielding Tensors Using Group Theory, MO Analysis, and Modern Density-Functional Theory. *Concepts Magn. Reson. Part A* **2009,** *34A*, 91–123.

(64) Willans, M. J.; Schurko, R. W. A Solid-State NMR and Ab initio Study of Sodium Metallocenes. *J. Phys. Chem. B* **2003,** *107*, 5144–5161.

(65) Rossini, A. J.; Schurko, R. W. Experimental and Theoretical Studies of ^{45}Sc NMR Interactions in Solids. *J. Am. Chem. Soc.* **2006,** *128*, 10391–10402.

(66) Ooms, K. J.; Bolte, S. E.; Baruah, B.; Choudhary, M. A.; Crans, D. C.; Polenova, T. ^{51}V Solid-State NMR and Density Functional Theory Studies of Eight-Coordinate Non-oxo Vanadium Complexes: Oxidized Amavadin. *Dalton Trans.* **2009,** 3262–3269.

(67) Bolte, S. E.; Ooms, K. J.; Polenova, T.; Baruah, B.; Crans, D. C.; Smee, J. J. ^{51}V Solid-State NMR and Density Functional Theory Studies of Vanadium Environments in V(*V*)O_2 Dipicolinic Acid Complexes. *J. Chem. Phys.* **2008,** *128*, 052317–052328.

(68) Ooms, K. J.; Bolte, S. E.; Smee, J. J.; Baruah, B.; Crans, D. C.; Polenova, T. Investigating the Vanadium Environments in Hydroxylamido V(*V*) Dipicolinate Complexes Using ^{51}V NMR Spectroscopy and Density Functional Theory. *Inorg. Chem.* **2007,** *46*, 9285–9293.

(69) Pooransingh-Margolis, N.; Renirie, R.; Hasan, Z.; Wever, R.; Vega, A. J.; Polenova, T. ^{51}V Solid-State Magic Angle Spinning NMR Spectroscopy of Vanadium Chloroperoxidase. *J. Am. Chem. Soc.* **2006,** *128*, 5190–5208.

(70) Huang, W. L.; Todaro, L.; Yap, G. P. A.; Beer, R.; Francesconi, L. C.; Polenova, T. ^{51}V Magic Angle Spinning NMR Spectroscopy of Keggin Anions $[PV_nW_{12-n}O_{40}]^{(3+n)-}$: Effect of Countercation and Vanadium Substitution on Fine Structure Constants. *J. Am. Chem. Soc.* **2004,** *126*, 11564–11573.

(71) Ooms, K. J.; Feindel, K. W.; Terskikh, V. V.; Wasylishen, R. E. Ultrahigh-Field NMR Spectroscopy of Quadrupolar Transition Metals: ^{55}Mn NMR of Several Solid Manganese Carbonyls. *Inorg. Chem.* **2006,** *45*, 8492–8499.

(72) Schafer, A.; Horn, H.; Ahlrichs, R. Fully Optimized Contracted Gaussian-Basis Sets for Atoms Li to Kr. *J. Chem. Phys.* **1992,** *97*, 2571–2577.

(73) Ooms, K.; Polenova, T.; Shough, A. M.; Doren, D. J.; Nash, M. J.; Lobo, R. F. Identification of Mixed Valence Vanadium in ETS-10 Using Electron Paramagnetic Resonance, ^{51}V Solid-State Nuclear Magnetic Resonance, and Density Functional Theory Studies. *J. Phys. Chem. C* **2009,** *113*, 10477–10484.

(74) Lauher, J. W.; Hoffmann, R. Structure and Chemistry of Bis(Cyclopentadienyl)−ML_n Complexes. *J. Am. Chem. Soc.* **1976,** *98*, 1729–1742.

(75) Larsen, F. H.; Lipton, A. S.; Jakobsen, H. J.; Nielsen, N. C.; Ellis, P. D. ^{67}Zn QCPMG Solid-State NMR Studies of Zinc Complexes as Models for Metalloproteins. *J. Am. Chem. Soc.* **1999,** *121*, 3783–3784.

(76) Lipton, A. S.; Buchko, G. W.; Sears, J. A.; Kennedy, M. A.; Ellis, P. D. ^{67}Zn Solid-State NMR Spectroscopy of the Minimal DNA Binding Domain of Human Nucleotide Excision Repair Protein XPA. *J. Am. Chem. Soc.* **2001,** *123*, 992–993.

(77) Lipton, A. S.; Sears, J. A.; Ellis, P. D. A General Strategy for the NMR Observation of Half-Integer Quadrupolar Nuclei in Dilute Environments. *J. Magn. Reson.* **2001,** *151*, 48–59.

(78) Lipton, A. S.; Heck, R. W.; Sears, J. A.; Ellis, P. D. Low Temperature Solid-State NMR Experiments of Half-Integer Quadrupolar Nuclides: Caveats and Data Analysis. *J. Magn. Reson.* **2004,** *168*, 66–74.

(79) Lipton, A. S.; Heck, R. W.; Primak, S.; McNeill, D. R.; Wilson, D. M.; Ellis, P. D. Characterization of Mg^{2+} Binding to the DNA Repair Protein Apurinic/Apyrimidic Endonuclease 1 via Solid-State ^{25}Mg NMR Spectroscopy. *J. Am. Chem. Soc.* **2008,** *130*, 9332–9341.

(80) Walter, T. H.; Turner, G. L.; Oldfield, E. ^{17}O Cross-Polarization NMR-Spectroscopy of Inorganic Solids. *J. Magn. Reson.* **1988,** *76*, 106–120.

(81) Vega, S. Multiple-Quantum Cross-Polarization NMR on Spin Systems with $I = 1/2$ and $S = 3/2$ in Solids. *Phys. Rev. A* **1981,** *23*, 3152–3173.

DOI: 10.1021/jz1012017 | *J. Phys. Chem. Lett.* **2010,** *1*, 2989–2998

(82) Rosay, M.; Tometich, L.; Pawsey, S.; Bader, R.; Schauwecker, R.; Blank, M.; Borchard, P. M.; Cauffman, S. R.; Felch, K. L.; Weber, R. T.; Temkin, R. J.; Griffin, R. G.; Maas, W. E. Solid-State Dynamic Nuclear Polarization at 263 GHz: Spectrometer Design and Experimental Results. *Phys. Chem. Chem. Phys.* **2010,** *12*, 5850–5860.

(83) Griffin, R. G.; Prisner, T. F. High Field Dynamic Nuclear Polarization — The Renaissance. *Phys. Chem. Chem. Phys.* **2010,** *12*, 5737–5740.

(84) Kentgens, A. P. M.; Verhagen, R. Advantages of Double Frequency Sweeps in Static, MAS and MQMAS NMR of Spin $I = 3/2$ Nuclei. *Chem. Phys. Lett.* **1999,** *300*, 435–443.

(85) Iuga, D.; Schafer, H.; Verhagen, R.; Kentgens, A. P. M. Population and Coherence Transfer Induced by Double Frequency Sweeps in Half-Integer Quadrupolar Spin Systems. *J. Magn. Reson.* **2000,** *147*, 192–209.

(86) Schurko, R. W.; Hung, I.; Widdifield, C. M. Signal Enhancement in NMR Spectra of Half-Integer Quadrupolar Nuclei via DFS-QCPMG and RAPT-QCPMG Pulse Sequences. *Chem. Phys. Lett.* **2003,** *379*, 1–10.

(87) Larsen, F. H.; Jakobsen, H. J.; Ellis, P. D.; Nielsen, N. C. Sensitivity-Enhanced Quadrupolar-Echo NMR of Half-Integer Quadrupolar Nuclei. Magnitudes and Relative Orientation of Chemical Shielding and Quadrupolar Coupling Tensors. *J. Phys. Chem. A* **1997,** *101*, 8597–8606.

(88) Arfken, G. *Mathematical Methods for Physicists*, 3rd ed.; Academic Press: New York, 1985.

(89) Rose, M. E. *Elementary Theory of Angular Momentum*; Wiley: New York, 1957.

(90) Eichele, K.; Wasylishen, R. E. WSolids: Solid-State NMR Simulation Package. In *WSolids1: Solid-State NMR Spectrum Simulation*; V1.17.28 ed.; University of Alberta: Edmonton, 2001.

(91) Bak, M.; Rasmussen, J. T.; Nielsen, N. C. SIMPSON: A General Simulation Program for Solid-State NMR Spectroscopy. *J. Magn. Reson.* **2000,** *147*, 296–330.

(92) Frisch, M. J.; Trucks, G. W.; Schlegel, H. B.; Scuseria, G. E.; Robb, M. A.; Cheeseman, J. R.; Montgomery, J., Jr.; Vreven, T.; Kudin, K. N.; Burant, J. C.; et al. *Gaussian 03*, revision B.03; Gaussian, Inc.: Pittsburgh, PA, 2003.

(93) McKenzie, T. C.; Sanner, R. D.; Bercaw, J. E. Crystal and Molecular-Structure of Bis(pentamethylcyclopentadienyl)-dichlorotitanium(*IV*). *J. Organomet. Chem.* **1975,** *102*, 457–466.

(94) Pevec, A. Crystal Structures of (η^5-C_5Me_5)$TiCl_3$ and (η^5-C_5Me_4H)$TiCl_3$. *Acta Chim. Slov.* **2003,** *50*, 199–200.

(95) Rossini, A. J.; Mills, R. W.; Briscoe, G. A.; Norton, E. L.; Geier, S. J.; Hung, I.; Zheng, S.; Autschbach, J.; Schurko, R. W. Solid-State Chlorine NMR of Group IV Transition Metal Organometallic Complexes. *J. Am. Chem. Soc.* **2009,** *131*, 3317–3330.

(96) Becke, A. D. Density-Functional Exchange-Energy Approximation with Correct Asymptotic-Behavior. *Phys. Rev. A* **1988,** *38*, 3098–3100.

(97) Becke, A. D. Density-Functional Thermochemistry. 3. The Role of Exact Exchange. *J. Chem. Phys.* **1993,** *98*, 5648–5652.

(98) Lee, C. T.; Yang, W. T.; Parr, R. G. Development of the Colle—Salvetti Correlation-Energy Formula into a Functional of the Electron-Density. *Phys. Rev. B* **1988,** *37*, 785–789.

(99) Woon, D. E.; Dunning, T. H. Gaussian-Basis Sets for Use in Correlated Molecular Calculations. 3. The Atoms Aluminum through Argon. *J. Chem. Phys.* **1993,** *98*, 1358–1371.

(100) Clark, S. J.; Segall, M. D.; Pickard, C. J.; Hasnip, P. J.; Probert, M. J.; Refson, K.; Payne, M. C. First Principles Methods Using CASTEP. *Z. Kristallogr.* **2005,** *220*, 567–570.

(101) Profeta, M.; Mauri, F.; Pickard, C. J. Accurate First Principles Prediction of ^{17}O NMR Parameters in SiO_2: Assignment of the Zeolite Ferrierite Spectrum. *J. Am. Chem. Soc.* **2003,** *125*, 541–548.

DOI: 10.1021/jz1012017 | *J. Phys. Chem. Lett.* **2010,** *1*, 2989–2998